ADBA Chaos and Fractals
Cutting-Edge Scientific Solutions

e-ISSN: 3023-8951
RESEARCH ARTICLE
Vol.2 / No.2 / 2025 / pp.38-42
https://doi.org/10.69882/adba.chf.2025072

Dynamical Analysis of Barium Titanate Crystal in Alternative Voltage RL Circuit

Guy Joseph Eyebe [*,1], **Justin Mibaile** [α,2], **Rolande Tsapla Fotsa** [β,3], **Gambo Betchewe** [§,4] **and Alidou Mohamadou** [§,5]

[*]Department of Oil and Gas Mechanical Engineering, National Advanced School of Mines and Petroleum Industries, P.O. Box 08, Kaele, Cameroon, [α]Department of Renewable Energy, National Advanced School of Engineering, University of Maroua, P.O. Box 46, Maroua, Cameroon, [β]Department of Mechanical Engineering, College of Technology, University of Buea, P.O. BOX 63, Buea, Cameroon, [§]Department of Physics, Faculty of Science, The University of Maroua, P.O. Box 814, Maroua, Cameroon.

ABSTRACT This brief paper theoretically investigates the dynamical characteristics of ferroelectric materials, specifically barium titanate $(BaTiO_3)$ crystal in alternative voltage resistor (R) and inductor (L) circuit. The theory of Landau-Ginzburg-Devonshire and Kirchhoff's law are used to derive the equation for the polarization field in the $BaTiO_3$ crystal. The Averaging method is applied to obtain an approximate analytical solution, and the numerical simulations of the system's equations is used to confirm the analytical obtained solution. The Melnikov method is used to investigate horseshoe chaos and the critical amplitude of excitation. The phase portraits, Poincaré sections, local maxima and greatest Lyapunov exponent are drawn to confirm the results obtained with Melnikov method.

KEYWORDS
Barium titanate crystal
Polarization
Averaging method
Melnikov method
Horseshoe chaos

INTRODUCTION

Ferroelectric materials are materials that exhibit spontaneous and reversible electrical polarization under the influence of an electric field. $BaTiO_3$ is an example of a ferroelectric material that has been extensively studied for its unique properties (Chen *et al.* 2018, 2024). The $BaTiO_3$ can be produced using various methods including room temperature synthesis, hydrothermal processes, bioinspired and biosynthetic approaches, sonochemical techniques, molten salt reactions, and peptide or phage-templated strategies, each enabling control over particle size, morphology, and phase with potential for green, scalable, and low-cost production (Chen *et al.* 2018, 2024). Chen *et al.* (2018) demonstrated that $BaTiO_3$ nanoparticles could be synthesized at room temperature conditions under ambient pressure. The hydrothermal synthesis of $BaTiO_3$ utilizing $NaTi_3O_6(OH) - (H_2O)_2$ nanowires, conducted by controlling temperature, alkalinity, and time was studied by (Chen *et al.* 2024).

Studies on the dielectric and ferroelectric properties of$BaTiO_3$ single crystals using the Landau phenomenological thermodynamic potential have been extensively conducted. Wang et *al*. suggested that when using the sixth-power free energy expansion of the thermodynamic potential, remarkably different values of the fourth-power coefficient are required to adequately reproduce the nonlinear dielectric behavior of the paraelectric phase and the electric field-induced ferroelectric phase, respectively (Wang *et al.* 2007). To develop the Landau-Devonshire potential of the perovskites $BaTiO_3$, the Gibbs free energy of $BaTiO_3$ single crystal has been expanded up to 10^{th}-order polynomial by (Ma *et al.* 2017). Large studies have shown that barium titanate crystals can be integrated into silicon and photonic platforms to enable high-performance, low-voltage, and high-speed electro-optic modulators and tunable dielectric devices for advanced integrated circuits and photonic applications. Picavet et *al*. presented a low-cost, high-throughput, and flexible method for integrating highly textured $BaTiO_3$ films on photonic integrated circuits, enabling large-scale fabrication of nanophotonic $BaTiO_3$ thin-film modulators (Picavet *et al.* 2024).

Xiong *et al.* (2014) showed how Ferroelectric $BaTiO_3$ thin films on silicon-on-insulator platforms has promising potential for broadband applications, with modulation bandwidth in the gigahertz regime. (Nayak *et al.* 2014) showed that $BaTiO_3$ multipods with high permittivity and low dielectric loss could be easily prepared and used for charge storage devices and electronic applications. Nonlinear dissipative dynamics, which underlie most real systems, have gained significant attention from theoretical and experimental researchers over the past few decades. Examples

Manuscript received: 21 May 2025,
Revised: 17 July 2025,
Accepted: 17 July 2025.

[1]yusufeyebe@gmail.com (**Corresponding author**)
[2]thejust7@yahoo.fr
[3]tsapla.fotsa@ubuea.cm
[4]gambobetch@yahoo.fr
[5]alidoumohamadou@gmail.com

of physical designs that are modeled by these dynamics include Josephson junctions, lasers etc.. A common characteristic of all these devices is that they can display surprisingly irregular behaviors when a control parameter is slightly modified. (Oikawa *et al.* 2024) analyzed chaotic behavior in Josephson junction for high-quality random-number generation. (Shuai *et al.* 2025) conducted research on chaos dynamic characteristics of multiple interactive Josephson junction application. (Kang *et al.* 2024) revealed a new scenario for the transition of solitons to chaos in a mode-locked fiber laser: The modulated subharmonic route.

The main reason justifying such interest lies in the fact that $BaTiO_3$ crystal is a good candidate for designing integrated circuits. The aim of this paper involves the determination of horseshoe chaos in the barium titanate crystal in alternative voltage RL circuit. Following this introduction, the paper is organized as follows: in section 2, we derive the governing equation of the circuit, the averaging method is applied to obtain an approximate analytical solution, and the numerical simulation of the system's equations is used to confirm the analytical results. The Melnikov method is used to investigate the Hamilton chaos, The phase portraits, Poincare sections, local maxima, and greatest Lyapunov exponent are drawn. Finally, section 3 is devoted to summarising the most important conclusions.

ANALYSIS OF $BaTiO_3$ CRYSTAL IN ALTERNATIVE VOLTAGE RL CIRCUIT

The $BaTiO_3$ crystal connected to alternative voltage RL circuit is considered in this paper (Figure 1). A simple case at temperatures in the vicinity of only the cubic-tetragonal phase transition where nonlinear behavior becomes stronger due to the strong nonlinearity of the restoring force and other effects and phase transitions (orthorhombic, rhombohedral) are negligible (Wang *et al.* 2007; Ma *et al.* 2017). We thus restrict the analysis in this paper to the case where the electromechanical coupling coefficient is very weak so that the dynamics of the electrical component is sufficient to capture all the properties of the system. The Landau model, completed by Devonshire (Coelho 1979; Waser and Lohse 1998; Starkov *et al.* 2022) thermodynamically describes the phase transitions by postulating that the free energy associated with the displacement of the dipoles in a crystal is a Taylor series development as a function of the the spontaneous polarization P. If we consider that it is subjected to an electric field, an additional energy term is added. Using Gibbs free energy of the $(BaTiO_3)$ crystal and Applying Kirchhoff's law, the equation for the polarization field in the crystal can be derived as

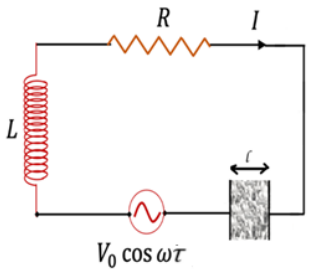

Figure 1 $BaTiO_3$ crystal connected to alternative voltage RL circuit.

$$U_R + U_L + U_{Crystal} = V_0 \cos \omega \tau, \tag{1}$$

with $U_R = RI(\tau) = R\frac{dq(\tau)}{d\tau}$, $U_L = L\frac{dI(\tau)}{d\tau} = L\frac{d^2q(\tau)}{d\tau^2}$, $U_{Crystal} = \left[\alpha(T)\bar{P} - \beta\bar{P}^3 + \gamma\bar{P}^5\right] l$, where $I(\tau)$ and $q(\tau)$ are electric current and charges. $\bar{P}$ is spontaneous polarization, R, L, l, A are respectively RL constants, width and surface of crystal. V_0 is amplitude of sinusoidal excitation with frequency w, α, β and γ are constant coefficients except α which depends on the temperature. The coefficient $(-\beta)$ instead of β is used in the equation to take into account its negative sign found in the literature (Wang *et al.* 2007; Ma *et al.* 2017). Equation (1) can be rewritten in the following form

$$\frac{d^2\bar{P}}{d\tau^2} + \frac{R}{L}\frac{d\bar{P}}{d\tau} + \frac{l}{LA}\left[\alpha(T)\bar{P} - \beta\bar{P}^3 + \gamma\bar{P}^5\right] = \frac{V_0}{A}\cos w\tau, \tag{2}$$

To put the equation (2) into a dimensionless form, let us use the rescaling :

$$\begin{aligned} &\omega_0 = \frac{\beta^2 l}{4\gamma LA}, t = \omega_0\tau, P = \bar{P}\sqrt{\frac{2\gamma}{\beta}}, \mu = \frac{R}{L\omega_0}, \\ &\alpha_T = \frac{l}{AL\omega_0^2}\alpha(T), \Omega = \frac{\omega}{\omega_0}, V = \frac{V_0}{AL\omega_0^2}\sqrt{\frac{2\gamma}{\beta}}. \end{aligned} \tag{3}$$

By substituting Eq. (3) in Eq. (2), it becomes :

$$\frac{d^2P}{dt^2} + \mu\frac{dP}{dt} + \alpha_T P - 2P^3 + P^5 = V\cos(\Omega t) \tag{4}$$

The potential energy associated with the system of Eq. (4) is

$$U(P) = \frac{1}{2}\alpha_T P^2 - \frac{1}{2}P^4 + \frac{1}{6}P^6 + C, \tag{5}$$

where C is a constant depending of characteristic potential. The shape of the potential given by Eq. (5) is shown in Figure 2 for different values of α_T.

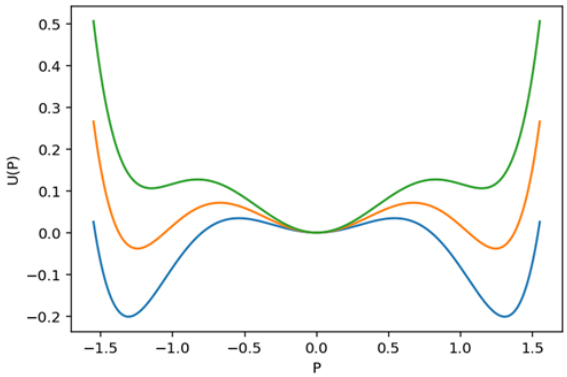

Figure 2 Shape of the potential for given value of α_T: (α_T =0.5 (blue), α_T =0.7 (red), α_T =0.9 (green)).

Figure 2 has three wells and two humps. By decreasing the value of α_T, the depth of three increase.

Averaging method

The averaging Method is used in this paper since the $BaTiO3$ crystal in Fig.1 is subjected to a weakly periodic forcing like an AC electric field, resulting in both rapid oscillations and slower changes due to the medium's nonlinear response. It effectively reduces the original system, which may be analytically intractable due to its nonlinearity and time dependence, into an averaged system that describes the slow evolution of amplitude and phase (Sanders *et al.* 2007). The averaging method is used in Eq. (4)

to obtain approximate solutions and confirm these mathematical results through numerical simulations of the system's equations. Figure 3 illustrates the curve of the amplitude of P versus frequency for both the analytical and numerical solutions. The solution can be written as

$$\begin{aligned} P(t) &= a(t)\cos(\theta(t)), \theta(t) = \sqrt{\alpha_T}t + \phi(t) \\ \frac{dP}{dt} &= -a(t)\sqrt{\alpha_T}\sin(\theta(t)), \end{aligned} \tag{6}$$

where a and θ represent the amplitude and the phase which are slow-varying functions of t. Substituting Eq. (6) into Eq. (4) and average over the period $T = 2\pi/\sqrt{\alpha_T}$, we obtain

$$\begin{aligned} \frac{da}{dt} &= -\frac{\mu}{2}a \\ \frac{d\phi}{dt} &= -\frac{3a^2}{4\sqrt{\alpha_T}} + \frac{5a^4}{16\sqrt{\alpha_T}}, \end{aligned} \tag{7}$$

By integrating each component of Eq. (7), it is obtained

$$\begin{aligned} a(t) &= a_0 \exp\left(\frac{-\mu t}{2}\right) \\ \phi(t) &= \phi_0 - \frac{3a_0^2}{4\mu\sqrt{\alpha_T}}\left(1 - \exp\left(\frac{-\mu t}{2}\right)\right) \\ &+ \frac{5a_0^4}{32\mu\sqrt{\alpha_T}}\left(1 - \exp\left(\frac{-2\mu t}{2}\right)\right). \end{aligned} \tag{8}$$

Now to confirm this mathematical result we apply numerical integration of Eq. (4) using robust four order Runge-Kutta and depict both numerical and analytical solutions.

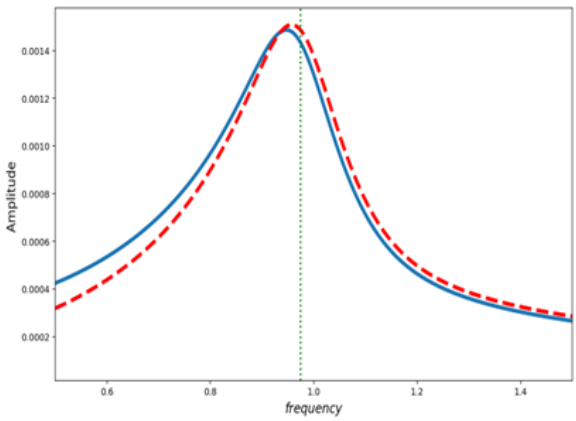

Figure 3 Amplitude versus frequency (analytical : Blue and numerical : Red).

Figure 3 shows in blue line, the variation of the amplitude of the solution (6) where a_0, ϕ_0 are constants. The curve in red is the same amplitude obtained from the numerical simulation of Eq. (4). One finds a good agreement between the mathematical and numerical results.

Melnikov method

To establish the conditions for the emergence of chaos in Eq. (4), the Melnikov method is applied (Melnikov 1963; Wiggins 1990). Consider the dynamical equation of a given system written in vector form

$$\dot{u} = g_0(u) + \varepsilon g_p(u,t), u = \left(P, \frac{dP}{dt}\right), \tag{9}$$

$$\begin{aligned} g_0(u) &= \begin{pmatrix} \frac{dP}{dt} \\ -\sqrt{\alpha_T}P + 2P^3 - P^5 \end{pmatrix}, \\ g_p(u,t) &= \begin{pmatrix} 0 \\ -\mu\frac{dP}{dt} + V\cos(\Omega t) \end{pmatrix}, \end{aligned} \tag{10}$$

where u is the state vector, g_0 is the vector field chosen with the non-perturbed Hamiltonian and g_p is a periodic perturbation function. Let's consider a Hamiltonian system that has saddle points connected by a separatrix or heteroclinic orbit, or possibly just a single hyperbolic saddle point with a homoclinic orbit. When a perturbation g_p is introduced, the orbits of the system become altered. If the perturbed and unperturbed manifolds intersect transversally, the geometry of the basin of attraction may turn fractal. This fractal structure indicates a high sensitivity to initial conditions, which is a proof of chaotic behavior. The Melnikov's theorem which gives the condition for the fractal basin boundary can be given as follows [9,10].

$$\begin{aligned} M(t_0) &= \int_{-\infty}^{+\infty} g_0(u(t)) \wedge g_p(u(t), t+t_0), \\ M(t_0) &= 0, \frac{dM(t_0)}{dt} \neq 0. \end{aligned} \tag{11}$$

The Hamiltonian of Eq. (3) is defined by

$$H_0(P, \frac{dP}{dt}) = \frac{1}{2}\left(\frac{dP}{dt}\right)^2 + \frac{\alpha_T}{2}P^2 - \frac{1}{2}P^4 + \frac{1}{6}P^6. \tag{12}$$

Given the shape of the potential U, one can make the assumption that the system possesses homoclinic orbits connecting saddle points and heteroclinic orbits connecting hyperbolic saddle points. The mathematical derivation of this Melnikov function can be found in (Tchoukuegno *et al.* 2002; Lenci *et al.* 1999) and Applying this Melnikov condition gives the following conditions for the appearance of chaos:

$$\begin{aligned} V_{cr}^{het} &\geq \left[\frac{(2\chi+1)}{(1-\chi^2)^{1/2}}\left(\sin^{-1}(\chi) + \frac{\pi}{2}\right) + 2 + \chi\right]. \\ &\frac{\mu P_u Y}{8\Omega\pi(\chi+1)}\sinh\frac{2\Omega}{Y}, \\ V_{cr}^{Ho} &\geq \left[\frac{(2\chi+1)}{(1-\chi^2)^{1/2}}\left(\sin^{-1}(\chi) - \frac{\pi}{2}\right) + (2+\chi)\right]. \\ &\frac{\mu P_u Y}{32\Omega\pi(\chi+1)}\frac{1}{\sinh\left(\frac{2\Omega}{Y}\right)}, \end{aligned} \tag{13}$$

$$Y = P_u^2\left(2\left(\rho^2 - 1\right)\right)^{1/2}, \chi = \frac{5-3\rho^2}{3\rho^2-1}, \rho = P_s/P_u.$$

where V_{cr}^{Ho} and V_{cr}^{het} are critical values of voltage respectively for homoclinic and heteroclinic orbits, Ps and Pu stand for stable and unstable equilibrium points. These conditions establish the threshold amplitudes of the supply voltage above which horseshoe chaos occurs. Figures 4 and 5 illustrate the conditions for homoclinic and heteroclinic orbits in the (Ω, V) plane for different values of α_T . The area above the line represents values of Ω and V that lead to unpredictable or chaotic behavior, while the area below the line corresponds to regular behavior.

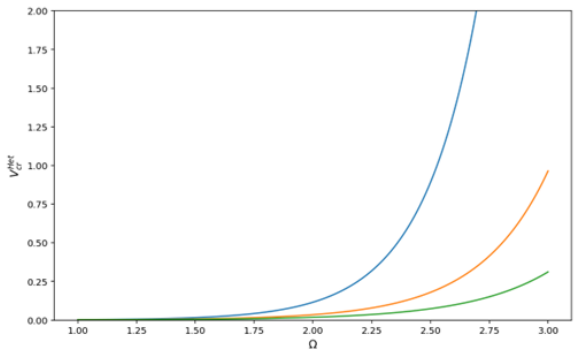

Figure 4 Critical value of voltage V_{cr}^{het} for given value of α_T : (α_T =0.3 (green), α_T =0.15 (red) and α_T =0.1 (blue)).

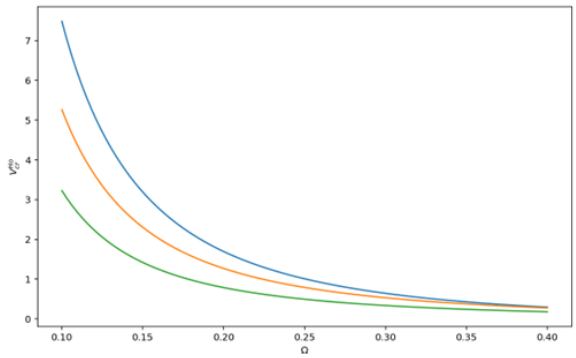

Figure 5 Critical value of voltage V_{cr}^{ho} for given value of α_T : (α_T =0.3 (green), α_T =0.15 (red) and α_T =0.1 (blue)).

In Figures 4 and 5, a variation of the critical value of voltage as a function of Ω are depicted. This is illustrated for different values of the parameter α_T. It is clear that the the critical value of ac- voltage in relation to Ω, which signifies the threshold for the onset of chaos, is significantly affected by the parameter α_T. As shown in Figure 4, a decrease in the parameter α_T results in a reduction of the chaotic domain for heteroclinic orbits. Figure 5 illustrates that a lower value of α_T enhances stability and narrows the chaotic region. To test the validity of these results, Fig. 6 is depicted, to confirm the analytical predictions of chaotic illustrated in Figs. 4 and 5. The phase portraits, Poincaré sections are depicted in Fig. 6, with parameters set to $\alpha_T = 0.04$, $\mu = 1.1$, $V = \Omega = 3.5$, $V = \Omega = 2.5$ with initial condition $(P(0) = 0.5, dP(0)/dt = 0.0)$. Figure 6 supports the validity of the analytical study presented in section 2.2 and visually represented in Figs. 4 and 5, demonstrating the presence of zones exhibiting chaotic and regular dynamics.

Figure 7 presents the local maxima of P and its corresponding greatest Lyapunov exponent (GLE) versus the parameter V.

Figure 7 (a) presents bistable limit cycle, period doubling route to chaotic region with windows of periodic characteristics, coexistence between limit cycle and chaotic characteristics and limit cycle, respectively. GLE of Figure 7 (b) confirms the dynamical characteristics found in Fig. 7 (a). The dynamical characteristics found in Fig. 7 are depicted in Fig. 8.

Bistable limit cycle is shown in Fig. 8 (a). Figures 8 (b) and (c) present two different shapes of chaotic characteristics. The coexistence between limit cycle and chaotic characteristics is illustrated in Fig. 8 (d).

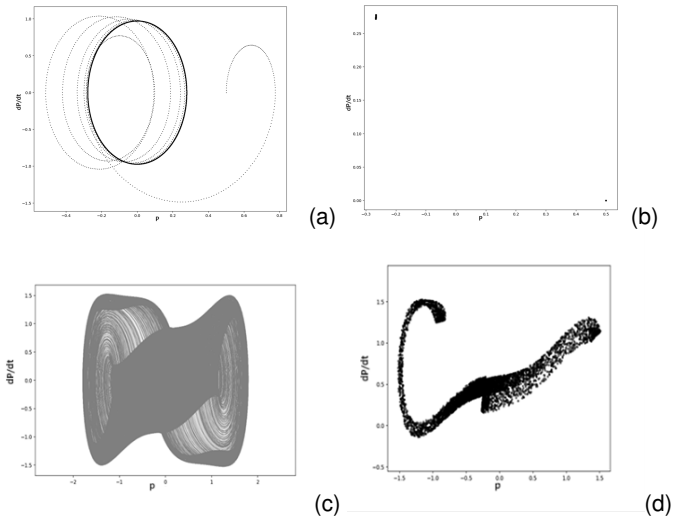

Figure 6 Phase portraits and Poincare sections $(\alpha_T = 0.04, \mu = 1.1)$: (a-b) $V = \Omega = 3.5$, (c-d) $V = \Omega = 2.5$. The curves are obtained by using the initial conditions $(P(0), dP(0)/dt) = (0.5, 0.0)$.

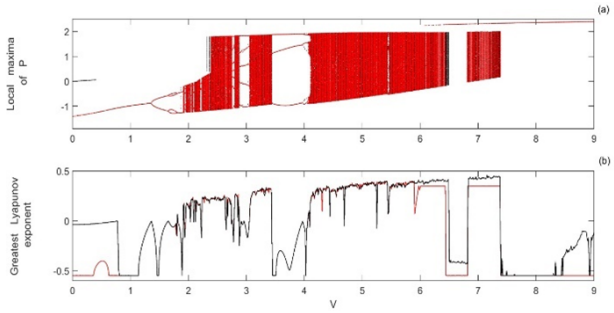

Figure 7 Local Maxima of P and its corresponding GLE versus the parameter V for $\alpha_T = 0.04$, $\mu = 1.1$ and $\Omega = 2.5$. Black dots (curves) are obtained by increasing the parameter V while red dots (curves) are obtained by decreasing the parameter V.

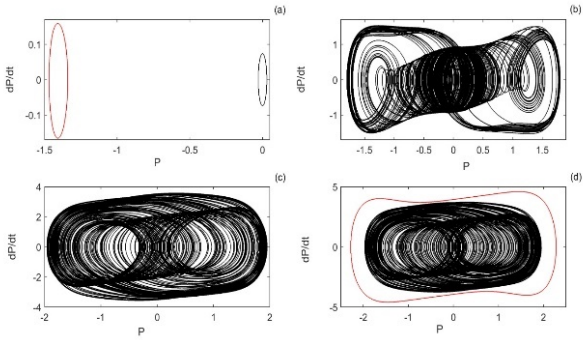

Figure 8 Phase portraits for given values of V $(\alpha_T = 0.04, \mu = 1.1)$: (a) $V = \Omega = 0.2$, (b) $V = \Omega = 2.5$, (c) $V = \Omega = 6$ and (d) $V = \Omega = 6.48$. The black curves are obtained by using the initial conditions $(P(0) = 0.01, dP(0)/dt = 0.01)$ while the red curves are obtained by using the initial conditions $(P(0) = 5.0, dP(0)/dt = 0.01)$.

CONCLUSION

This paper investigated dynamical characteristics in barium titanate crystal in alternative voltage RL circuit using the averaging method, Melnikov method and numerical simulations. The averaging method was applied to obtain an approximate analytical solution and the numerical simulations of the system's equations was used to confirm the analytical results. Good agreement between the analytical and numerical results was found. The Melnikov was demonstrated that the critical values of alternative voltage which delimits the boundary between chaotic and non-chaotic regimes is dependent to the structural parameter of the crystal. Numerical verifications using phase plots, Poincaré maps, local maxima and the greatest Lyapunov exponent supported the analytical prediction of chaotic behavior. This study yielded practical design information for chaos-resistant integrated circuits. Generalization of this study to also include the thermal-dependent part of circuit is needed for the further development of chaos control in complex circuits.

Ethical standard

The authors have no relevant financial or non-financial interests to disclose.

Availability of data and material

Not applicable.

Conflicts of interest

The authors declare that there is no conflict of interest regarding the publication of this paper.

LITERATURE CITED

Chen, S., B. Han, X. Chen, F. Xu, and G. Wang, 2024 Hydrothermal synthesis and morphology control mechanism of $batio_3$ from $nati_3o_6(oh)(h_2o)_2$ precursors. Ceramics International **50**: 21779–21787.

Chen, T., J. Meng, S. Wu, J. Pei, Q. Lin, *et al.*, 2018 Room temperature synthesized $batio_3$ for photocatalytic hydrogen evolution. Journal of Alloys and Compounds **754**: 184–189.

Coelho, R., 1979 *Physics of dielectrics for Engineers*. Elsevier Scientific Publishing Company, Amsterdam.

Kang, H., A. Zhou, Y. Zhang, X. Wu, B. Yuan, *et al.*, 2024 Observation of optical chaotic solitons and modulated subharmonic route to chaos in mode-locked laser. Physical Review Letters **133**: 263801.

Lenci, S., G. Menditto, and A. Tarantino, 1999 Homoclinic and heteroclinic bifurcations in the non-linear dynamics of a beam resting on an elastic substrate. International Journal of Non-Linear Mechanics **34**: 615–632.

Ma, Z., L. Xi, H. Liu, F. Zheng, H. Gao, *et al.*, 2017 Ferroelectric phase transition of $batio_3$ single crystal based on a tenth order landau-devonshire potential. Computational Materials Science **135**: 109–118.

Melnikov, V., 1963 On the stability of the center for some periodic pertubations. Trans. Moscow Math. Soc. **12**: 1–57.

Nayak, S., B. Sahoo, T. Chaki, and D. Khastgir, 2014 Facile preparation of uniform barium titanate ($batio_3$) multipods with high permittivity: impedance and temperature dependent dielectric behavior. RSC Advances **4**: 1212–1224.

Oikawa, D., H. Komatsu, K. Tsuzuki, H. Andoh, and T. Tsukamoto, 2024 Chaotic behavior in josephson junction for high-quality random-number generation. Journal of Applied Physics **136**: 123909.

Picavet, E., E. Lievens, K. De Geest, H. Rijckaert, E. Fernandez, *et al.*, 2024 Integration of solution-processed $batio_3$ thin films with high pockels coefficient on photonic platforms. Advanced Functional Materials **34**: 2403024.

Sanders, J. A., F. Verhulst, and J. Murdock, 2007 *Averaging methods in nonlinear dynamical systems*. Springer Science and Business, New York.

Shuai, W., W. Litian, X. Yulong, L. Dan, and L. Xueming, 2025 Research on chaos dynamic characteristics of multiple interactive josephson junction application. AIP Advances **15**: 035336.

Starkov, I. A., M. A. Mishnev, and A. S. Starkov, 2022 The equation of state for metal-doped ferroelectrics within the weiss model. Journal of Advanced Dielectrics **12**: 2250011.

Tchoukuegno, R., B. N. Nbendjo, and P. Woafo, 2002 Resonant oscillations and fractal basin boundaries of a particle in a ϕ^6 potential. Physica A: Statistical Mechanics and its Applications **304**: 362–378.

Wang, Y., A. Tagantsev, D. Damjanovic, N. Setter, V. Yarmarkin, *et al.*, 2007 Landau thermodynamic potential for $batio_3$. Journal of Applied Physics **101**: 104115.

Waser, R. and O. Lohse, 1998 Electrical characterization of ferroelectric, paraelectric, and superparaelectric thin films. Integrated Ferroelectrics **21**: 27–40.

Wiggins, S., 1990 *Introduction to the applied Nonlinear dynamic systems and chaos*. Springer, New York.

Xiong, C., W. Pernice, J. Ngai, J. Reiner, D. Kumah, *et al.*, 2014 Active silicon integrated nanophotonics: ferroelectric $batio_3$ devices. Nano letters **14**: 1419–1425.

How to cite this article: Eyebe, G. J., Mibaile, J., Fotsa, R. T., Betchewe, G., and Mohamadou, A. Dynamical Analysis of Barium Titanate Crystal in Alternative Voltage RL Circuit. *Chaos and Fractals*, 2(2), 38-42, 2025.